The Rayleigh-like collapse of a conical bubble

T. G. Leighton, B. T. Cox, and A. D. Phelps
Institute of Sound and Vibration Research, University of Southampton, Southampton SO17 1BJ, United Kingdom

(Received 1 June 1998; revised 24 February 1999; accepted 2 July 1999)

Key to the dynamics of the type of bubble collapse which is associated with such phenomena as sonoluminescence and the emission of strong rebound pressures into the liquid is the role of the liquid inertia. Following the initial formulation of the collapse of an empty spherical cavity, such collapses have been termed ''Rayleigh-like.'' Today this type of cavitation is termed ''inertial,'' reflecting the dominant role of the liquid inertia in the early stages of the collapse. While the inertia in models of spherical bubble collapses depends primarily on the liquid, experimental control of the liquid inertia has not readily been achievable without changing the liquid density and, consequently, changing other liquid properties. In this paper, novel experimental apparatus is described whereby the inertia at the early stages of the collapse of a conical bubble can easily be controlled. The collapse is capable of producing luminescence. The similarity between the collapses of spherical and conical bubbles is investigated analytically, and compared with experimental measurements of the gas pressures generated by the collapse, the bubble wall speeds, and the collapse times. © *2000 Acoustical Society of America.* [S0001-4966(90)00301-0]

PACS numbers: 43.25.Yw, 43.35.Ei [DLB]

INTRODUCTION

This paper compares experimental results with the predictions of an analysis for the collapse of a conical bubble, which adapts to a conical geometry the pioneering formulations of Rayleigh[1] and Noltingk and Neppiras.[2,3] Rayleigh considered the collapse of an empty cavity that remains spherical at all times, located in an incompressible liquid. The empty cavity is envisaged to be formed at rest ''as if a spherical portion of the fluid is suddenly annihilated'' [4] and, because of the hydrostatic pressure in the liquid, subsequently collapses. The wall speed becomes undefined as the radius approaches zero, a singularity that can be resolved by incorporating some permanent gas within the cavity.[1] Noltingk and Neppiras[2,3] incorporated this model of the collapse phase into a scheme in which the bubble first grows isothermally from an initial equilibrium size, subsequently undergoes adiabatic collapse, and then oscillates between maximum and minimum sizes (the addition of damping would cause the amplitude and period of these oscillations to decrease in time). Such so-called ''inertial'' collapses (reflecting the importance of the liquid inertia) were experimentally associated with the emission of liquid shocks at rebound, and the generation of sonoluminescence. Although theory has advanced considerably beyond the adiabatic models[5,6] (in line with developments in the observation of single-bubble sonoluminescence[7,8] and the issues it raises[9–14]), the transparency of the early models[1–3] has here been exploited to discuss the dynamics of conical bubbles, in a system where it is possible to modify the liquid inertia. The gas and liquid pressures can be measured, and the collapsing bubble wall photographed. The results are compared with a theory that adapts the analysis of Rayleigh, now more than 80 years old, for the inertial collapse of a conical bubble.

I. MATERIAL AND METHODS

A. Apparatus

Figure 1 shows the apparatus in which a gas pocket collapses into an otherwise liquid-filled conical hollow (of half-angle $\theta = 30$ degrees). Milled from polymethylmethacrylate (PMMA), the hollow has a circular horizontal cross section, 60-mm diameter at its base where it connects flush onto a steel U-tube. This is partially filled with degassed water at 15–17 °C, which can flow from the tube into the cone. At equilibrium, under ~0.1 MPa static pressure, a gas bubble of millimeter-order radius sits at the top of the cone. Then the top-plate is closed and the pumping train activated, reducing the static pressure in the tube so that the bubble undergoes relatively slow growth. After the bubble has expanded to the required size, the spring-loaded top-plate is opened. A pressure pulse of approximately 0.1 MPa propagates down the U-tube, causing the collapse of the bubble. The signal from an accelerometer on the top-plate provides the trigger for the various data acquisition systems (see below). The conical geometry not only allows the imaging of a ''cross section'' of the luminescing bubble ($45\% \pm 5\%$ of photons produced at the tip reaching the cone exterior). It also allows the positioning of pressure transducers within the gas, and within the surrounding liquid, since the center of the collapse is well defined. Define the variable ''bubble radius'' R_c as the vertical distance from the cone apex to the meniscus. Because the cross-sectional area in the cone increases with distance from the apex (r_c), the flow velocity of the liquid (of density ρ, assumed to be incompressible) decreases in proportion. Equating the flux at the position of the meniscus ($r_c = R_c$) to that across some cross section of the cone below it gives

$$\dot{R}_c dt \pi R_c^2 \tan^2\theta = \dot{r}_c dt \pi r_c^2 \tan^2\theta \Rightarrow \dot{R}_c/\dot{r}_c = (r_c/R_c)^2. \quad (1)$$

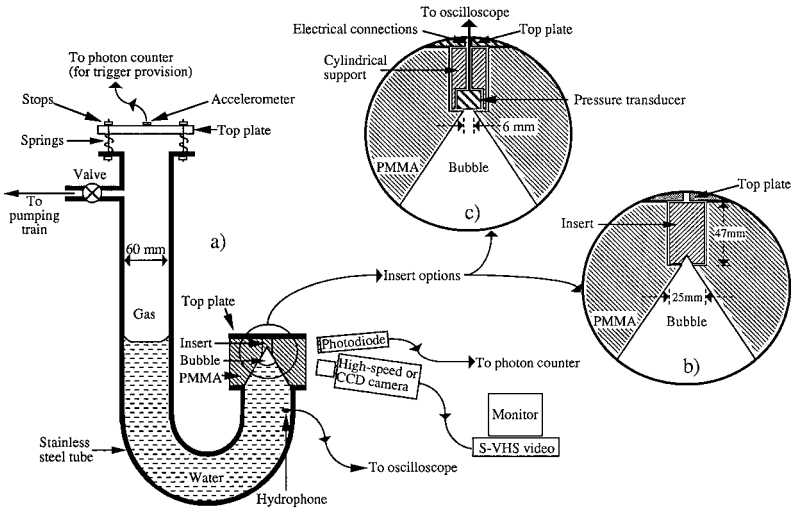

FIG. 1. (a) Diagram of the apparatus. (b) Insert showing the detail of the cone tip. (c) Insert showing detail of truncated cone, used for mounting pressure transducer.

Hence the liquid flow in the cone diverges and converges as in spherically symmetric conditions, within the limitations of the model (the actual nature of the flow is discussed in Sec. I B). In contrast, the flow in the U-tube has approximately one-dimensional geometry. This means that the inertia of the liquid is proportional to the length of fluid in the pipe.[15] Therefore, unlike the spherically symmetric case, the inertia does not converge to a finite value as one takes into account fluid at increasing distances from the bubble center. So by increasing the length of liquid in the U-tube, the inertia associated with the bubble collapse can be greatly increased.[16]

Optical instruments were deployed to study the collapse. A single frame was always taken with a stills camera immediately prior to the opening of the plate, in order to record the maximum bubble radius. Luminescence was monitored using a photon counting module (EG&G SPCM-200), which used a cooled avalanche silicon photodiode, and emitted a Transistor-Transistor Logic (TTL) pulse on detection of a photon. These were counted by a multi-channel scaler (EG&G T914P). The dark current was 25 counts/second. The counter was triggered by the accelerometer on the top-plate. Even when not required for photon counting, this system was always in use since, on receipt of the top-plate accelerometer signal, it provided the TTL signal which triggered the oscilloscope and provided a time marker for the high-speed film (see below).

During the photon counting, images of the luminescence were taken using a CCD camera (Photonic Science DS800). Operating at 25 f.p.s. (frames per second), it interlaced two fields, each of 40-ms duration but 20 ms out of phase (see Ref. 17 for details of exposure, persistence, video recording, etc.). High-speed images were taken of the bubble collapse using a Kodak Ektapro EM high-speed digital video camera. It could film at up to 1000 f.p.s. full-frame, or at 6000 f.p.s. with each frame occupying $\frac{1}{6}$ of the image screen. The top-plate accelerometer signal triggered a single flash signal, which allowed a common time basis between the film and the pressure signals, described below.

Because of their different ambient light requirements, the two camera systems could not be deployed simultaneously. However, instrumentation to measure the pressure of the liquid could be used simultaneously with each of them. These instruments were mounted in the 62-mm-tall PMMA extension to the shorter leg of the U-tube [Fig. 1(a)]. Within this extension, a pressure transducer (Bruel and Kjaer 8103 hydrophone), its center 10 cm below the apex of the cone, recorded the pressure fluctuations within the liquid. This system replaced the one used by Leighton *et al.*[17,18] which was prone to damage. Both systems could detect the rebound pressure pulses emitted by the bubble. (However, only the B&K 8103 system used here could be guaranteed to measure the amplitude of the rebound pressure pulses, since the amplitudes of these were beyond the range of the calibration available for the sensor used previously.[17]) Both systems could detect the reflections of these pressure pulses from the ends of the water column. However, unlike the sensor used by Leighton *et al.*,[17,18] the more robust Bruel and Kjaer device was not capable of measuring the pressure wave which propagates through the U-tube in response to the opening of the plate. According to the manufacturers, this hydrophone should behave linearly up to 4 MPa. Its calibration was checked regularly during the experiments and was stable to $\pm 0.5\%$. The spatial variation in the pressure pulses can be examined by the use of multiple sensors.[19]

The apex of the cone was itself designed to take two types of polycarbonate insert (described fully by Leighton *et al.*[17]), of 47-mm length and 25-mm outer diameter. The first [Fig. 1(b)] simply continues the conical hollow to the apex (and was used for all the results here except those of Fig. 8). If a collapse damaged the apex, it was easily replaced. The second type of insert [Fig. 1(c)] truncates the cone 5.25 mm before the apex by placing there a transducer (Keller PA-8, having 30-kHz resonance) which the manufacturers calibrate up to 100 MPa. However, here only the central circular area (6.05-mm diameter) of the full 13.0-mm-diam face of the transducer is exposed, and so an appropriate correction factor had to be employed in the measurement of gas pressure.[18] A third type of insert, not shown here, allows electrochemical sensors to be placed at the apex. These can monitor the regrowth of an oxide layer on an electrode there following its erosion by the collapse.[20] This allows measurement of the effects of erosion on a millisecond time scale.

The use of a U-tube with a conical termination was pioneered by Henwood and co-workers (Kosky and Henwood[19]

and Hawtin *et al.*[21]). It was used, however, to study a very different form of bubble activity: the condensation and oscillation of vapor bubbles. They had a particular interest in pressure transients, because of the implications for the generation and detection of accidental subcooled boiling in liquid-metal-cooled nuclear reactors. They photographed the vapor bubble, and recorded pressure transients along the length of the U-tube. Data from the system was compared with a model of the collapse of such vapor cavities by Hawtin *et al.*[21]

The theory and experiments reported in these earlier studies[19,21] are very different from the work reported here. In both cases it is the pressure difference exerted at the opposite ends of the water column that drives the motion. However, in the model used by Hawtin *et al.*[21] the pressure on the ''bubble wall'' is determined by the vapor pressure. In the current study the pressure is determined by the permanent gas, and the motion dominated by the inertia associated with the liquid.[18]

Hawtin *et al.*[21] concentrated on making measurements at higher temperatures, where the cavity dynamics are very different from the violent collapses studied here. For example, at temperatures in excess of 75 °C, they found that the pressure at the cone apex rose and fell relatively gently, over amplitudes of atmospheric order and time scales of around 50 ms, the rises coinciding with the contraction of the cavity and the falls with its expansion. The minimum bubble ''radius,'' achieved at the end of the compression phase, was in excess of 7 cm. This is the oscillation of a vapor cavity, and not an inertially dominated cavitation collapse of the type studied here. Inertia will in fact become a key factor at temperatures below ~55 °C, and Hawtin *et al.*[21] reported several difficulties in making observations in this lower temperature regime. These included the failure to find vapor cavities of an observable size at the first rebound below 69 °C (their theory had suggested this would be possible down to 50 °C), and to make measurements of the tip pressures below ~55 °C.

Summarizing their findings, Hawtin *et al.*[21] compare their theory against observations of tip pressures (<15 MPa), and collapse times (>30 ms), which are smaller and slower (respectively) than those found in the current study by around an order of magnitude. The minimum ''radius'' attained by their bubbles, at the end of the first collapse is, by comparison with the current study, very large (>5 cm). Measurements of these three parameters agree with their theory only for liquid temperatures in excess of ~60 °C.

The problems encountered by Hawtin *et al.*[21] when attempting to study and model their system at lower temperatures are not unexpected. Hawtin *et al.*[21] state that their theory cannot, for example, predict maximum pressures if the precollapse vapor pressure is below about 15 kPa. They give the reason as being the inapplicability of simple incompressible hydrodynamics when the collapse becomes more violent. It should be noted that 15 kPa corresponds to the vapor pressure of water at ~55 °C (the vapor pressure at the temperatures of the current study being roughly 1.7 kPa).[22] The theory outlined in the following section also assumes an incompressible liquid, but, by balancing the kinetic energy of the liquid with the work done by the liquid pressure and a permanent gas component, it can be compared with inertially dominated collapses at room temperature.

B. Analysis

Consider the following idealized bubble history. All the experiments begin with the injection of a small bubble into the cone, via a flexible pipe that is then removed, the topplate remaining open to the atmosphere. Buoyancy causes the bubble to sit close to the cone apex, and prior to growth the bubble is sufficiently small to remain approximately spherical (with radius R_f). The ambient pressure (comprising atmospheric, hydrostatic, and Laplace components), and the gas pressure inside the bubble, are in equilibrium. The partial vacuum is applied, and the bubble grows to a maximum radius of R_i (defined as the vertical distance from the cone apex to the meniscus). At this time, the internal gas pressure is $p_{g,i}$. A still photograph is taken, recording R_i, and then the vacuum released. A pressure pulse travels down the U-tube. On reaching the bubble wall, it reflects back along the pipe, towards the flat meniscus at the top of the long leg of the U-tube. The bubble collapses into the cone, the increasing gas pressure eventually slowing the collapse. When the bubble reaches minimum radius $R_{\min}$ with maximum internal pressure $p_{g,\max}$, rebound occurs, and a pressure pulse is emitted down into the liquid. As with the initial pressure step, all the rebound pulses continually recross the tube, reflecting from either end, until dissipated.[17] The bubble expands to a maximum size, then collapses again. If there were no dissipation, this process would repeat endlessly, the bubble always achieving the same maximum and minimum sizes (with the same maximum gas pressures), and the time between the emission of rebound pressure pulses would be constant. Damping causes the amplitude of oscillation, and the time between rebounds, to decrease steadily, such that in the end a small spherical bubble is undergoing small-amplitude, linear pulsations near the cone apex. If there is no mass loss or gain from the bubble, and the ambient conditions are the same as those prior to the imposition of the vacuum, then that bubble will have radius R_f. In practice, the bubble fragments after its first rebound, although (because of subsequent coalescence and collective behavior of the fragments) continued growth/collapse cycles do occur which resemble the behavior that would be expected of a bubble which did not fragment.[17,18] The nature of these cycles will be explored in more detail in this paper.

The analysis[18] concentrates on the initial growth, and the first collapse up until the bubble reaches minimum size. Although the meniscus is assumed to be flat throughout, it is not difficult to adapt the calculation for a curved meniscus, though this is less relevant to the precollapse conditions. The analysis considers the energy balance before and after the start of the collapse. The increase of kinetic energy of the liquid in the tube and cone must be equal to the work done by the gas at the interface as the bubble collapses, and the radius reduces from its precollapse value, $R_c = R_i$. At the start of the collapse, when $R_c = R_i$ and $\dot{R}_c = 0$, the gas within the bubble has pressure $p_{g,i}$ and temperature T_i. If there is no heat flow across the bubble wall (which is valid if the

collapse speed is fast), the gas pressure p_g and bubble volume follow an adiabatic relationship. Balancing the energies during the collapse in the manner outlined above gives an expression for the speed of the bubble wall:

$$\dot{R}_c^2=\frac{\left(\frac{r_{\max}}{R_c}\right)^4\frac{\pi\tan^2\theta}{3}\left[p_L(R_i^3-R_c^3)-\frac{p_{g,i}R_i^3}{(\gamma-1)}\left(\left(\frac{R_i}{R_c}\right)^{3(\gamma-1)}-1\right)\right]}{\frac{1}{2}\rho A_0\left[\left(\frac{1}{R_c}-\frac{1}{r_{\max}}\right)r_{\max}^2+\left(h_i-\frac{1}{A_0}\frac{\pi}{3}\tan^2\theta(R_i^3-R_c^3)\right)\right]}, \tag{2}$$

where $r_{\max}=52$ mm is the vertical distance from the apex to the base of the cone (where the cross-sectional area is $A_0=2.8\times10^{-3}\,\mathrm{m}^2$, the same as that in the U-tube), γ is the ratio of the specific heat of the gas at constant pressure to that at constant volume, and p_L is the pressure in the liquid at the bubble wall.

The numerator in Eq. (2) represents the energy terms from the work done by the liquid and the gas. The $\dot{R}_c^2 \propto(r_{\max}/R_c)^4$ dependence arises naturally from the inverse square divergence with distance of the liquid particle velocity in the cone [Eq. (1)]. Since $p_{g,i}$ represents the initial pressure of the gas in the bubble, the terms in Eq. (2) with which it is multiplied account for the work done by the bubble gas on the liquid. The other term in the numerator of Eq. (2) represents the work done by the liquid pressure, p_L.

The denominator in Eq. (2) is the inertia multiplied by a factor of $\frac{1}{2}$. Multiplying it by $\dot{R}_c^2$ gives the kinetic energy term in the energy balance which Eq. (2) represents. The first term in the denominator represents the inertia of the liquid in the cone; and the second, that of the liquid in the tube. The symbol h_i represents the initial length of liquid in the U-tube. As the collapse proceeds, liquid flows from the tube into the cone (the length of liquid in the column at the end of the collapse is about 2 cm shorter than its initial value). This reduces the inertia of the liquid remaining in the U-tube, and the expression following h_i in Eq. (2) corrects for this.

Therefore if $p_{g,i}$ in Eq. (2) is set to zero, and the gas content of the bubble is effectively removed, this would give an expression for $\dot{R}_c^2$ which would be obtained were the conical bubble to collapse in the manner of a Besant cavity, as characterized by Rayleigh for the spherical bubble.[1] It is not possible to generate a formulation for the collapse time through integration of Eq. (2) in the way that Rayleigh did for the spherical cavity. However, the collapse times predicted from Eq. (2) can be calculated numerically for both empty and gas-filled cavities, and compared with experimental measurements (see Sec. II). The collapse time is given by

$$t_{\mathrm{coll}}=\int_{R_{\min}}^{R_i}\frac{dR_c}{\dot{R}_c}, \tag{3}$$

which was calculated numerically using a routine based on Simpson's midpoint rule.

As described earlier, the conical bubble starts the collapse with a zero wall velocity and a maximum radius R_i, the gas within the bubble having pressure $p_{g,i}$ and temperature T_i. The wall velocity will next be zero at the minimum radius $R_{\min}$, when the pressure and temperature of the gas within the bubble are at a maximum, $p_{g,\max}$ and $T_{\max}$, respectively. Assuming no break-up, the bubble will then rebound to a maximum size of $R_{\max}$ which, if there are no losses, will also equal R_i. The positions of maximum and minimum radius are found by setting $\dot{R}_c=0$ in Eq. (2), such that

$$\left[p_L(R_i^3-R_c^3)-\frac{p_{g,i}R_i^3}{(\gamma-1)}\left(\left(\frac{R_i}{R_c}\right)^{3(\gamma-1)}-1\right)\right]=0 \qquad (R_c=R_{\max},R_{\min}). \tag{4}$$

As expected, one solution to Eq. (4) gives the position of $R_{\max}=R_i$, the initial radius. The other solution occurs at $R_c=R_{\min}$. Simple estimates in the limit of $R_{\min}\ll R_i$ can be made by simplifying Eq. (4), to give

$$R_{\min}=R_i\left(\frac{p_{g,i}}{p_L(\gamma-1)}\right)^{1/3(\gamma-1)}. \tag{5}$$

The only value which is unknown in this expression is $p_{g,i}$, the initial gas bubble pressure. Provided mass transfer across the bubble wall is negligible, $p_{g,i}$ can be estimated from the final, postcollapse conditions, as follows. As described above, after the plate has been released and all the energy has been dissipated from the collapse, experimental observations have shown a spherical bubble lying at rest just below the tip of the cone. The differences in state between this bubble and the initial bubble (before plate opening) are governed by an isothermal relationship in volume and pressure, as both states will be at the initial temperature T_i. Hence,

$$p_{g,i}\frac{\pi}{3}R_i^3\tan^2\vartheta=p_L\frac{4}{3}\pi R_f^3\Rightarrow p_{g,i}=\frac{4}{\tan^2\vartheta}\left(\frac{R_f}{R_i}\right)^3p_L, \tag{6}$$

where R_f is the spherical radius of the final bubble in the cone tip. It is assumed that the static liquid pressure on the bubble prior to growth equals the pressure step p_L which collapses the bubble. Equation (6) ignores the contribution to the internal pressure of the bubble due to the difference in height of the liquid in the two legs of the U-tube, and also any contribution due to the Laplace pressure (which, for a 1-mm-radius bubble, will be ~0.1% of the static pressure contribution). A more complete form of the theory, which includes the height difference, predicts that there is a negligible change in the collapse conditions from the approximate version considered here.

However, although the estimate for $R_{\min}$ calculated from the assumption that $R_{\min}\ll R_i$ described in Eq. (5) is valid for large initial meniscal displacements, a more exact solution is available through calculation of $R_{\min}$ iteratively using Newton–Raphson's method. This is done by Leighton

et al.,[18] who showed that as the initial bubble size becomes smaller, Eq. (5) overestimates $R_{\min}$, compared to the predictions of the iterative calculation. This becomes important in calculating the maximum tip pressures, and the more complete form is used in the calculations presented in this paper. The maximum pressure achieved in the collapse, at a time when $R_c = R_{\min}$, can be found from assuming the collapse to be adiabatic, and using the expression for $p_{g,i}$ derived in Eq. (6):

$$p_{g,\max} = p_{g,i}\left(\frac{R_i}{R_{\min}}\right)^{3\gamma} = \left[\frac{4}{\tan^2\vartheta}\left(\frac{R_f}{R_i}\right)^3\right]^{1/(1-\gamma)}[(\gamma-1)]^{\gamma/(\gamma-1)}p_L. \quad (7)$$

Following the same reasoning and approximations, the maximum temperature reached in the bubble can be expressed as

$$T_{\max} = T_i\left(\frac{R_i}{R_{\min}}\right)^{3(\gamma-1)} = \left[\frac{4}{\tan^2\vartheta}\left(\frac{R_f}{R_i}\right)^3\right]^{-1}(\gamma-1)T_i. \quad (8)$$

This model, therefore, begins with an adaptation of the 1917 Rayleigh calculation, and then incorporates a permanent gas phase with an isothermal growth stage and an adiabatic collapse, which dates from the Noltingk–Neppiras model of the 1950s. The analysis will be compared with experimental observations in a system where direct visual observation is possible of both growth and collapse, where the precollapse bubble size can be controlled, and where pressure sensors can be placed within the bubble gas and within the liquid outside the bubble wall.

The emphasis is to show how far this historical analysis can be taken in predicting the bubble dynamics in this novel situation. There are clear approximations. The liquid is assumed to be incompressible. The vapor is ignored, and (as shown by Hawtin *et al.*[21]) this will have a role in certain circumstances. The tip pressure is assumed to be generated by gas compression and not, for example, by liquid impact. The Reynolds number for the flow in the pipe ($\mathrm{Re} = \rho d u/\eta$, where $d = 0.06$ m is the pipe diameter and u is the flow velocity there) takes a maximum value of $\sim 10^5$ (Fig. 5). This indicates turbulent conditions. Combining this with the wall roughness allows the pressure loss resulting from wall friction to be estimated[23] at around 250 Pa, which is small compared with both the 0.1-MPa pressure which initiates bubble collapse and the bubble gas pressures which retard it.

II. RESULTS

A. High-speed photography

Figures 2 and 3 show a selection of 16 frames from a consecutive sequence of 305, filmed at 1000 f.p.s. (each frame occupying full screen). In discussing the collapse shown here, attention will be paid to the highlights that appear in the cone as a result of reflection and refraction of the backlighting. This is because in Fig. 4, a sequence filmed at 6000 f.p.s., the use of similar highlights is necessary to locate the features in these more complicated images. Figure 2(b) is a frame-by-frame schematic illustration to assist in the identification of features in Fig. 2(a) [and Fig. 3(b) similarly relates to Fig. 3(a)]. The first highlight is indicated in frame 1, arrowed in Fig. 2(a) and labeled in Fig. 2(b). This frame corresponds to the precollapse phase, when the bubble fills the entire region of the cone shown in the figure. The highlight is a white line, aligned with the cone axis, extending from ~1 mm below the cone tip down to ~5 mm below the cone tip. The appearance of the apex highlight can be used to qualitatively distinguish between two states. If it is visible, the top 5 mm of the cone contains a coherent gas pocket that fills the apex to a sufficient degree (Fig. 2 frames 1–3, 15–16; Fig. 3, frame 25). If it is not visible, this region accommodates enough water to be described as containing either ''clear water'' (a loose description of water having a low void fraction), or ''bubbly water'' (water having a high void fraction), or a coherent gas pocket which is insufficient to generate the highlight (Fig. 3, frame 305). If the apex highlight is indeed absent, further evidence is required to distinguish between these three options.

Similarly, in the bottom half of frame 1, there is a broader axial vertical white line [arrowed in Fig. 2(a) labeled in Fig. 2(b)]. This ''bottom highlight'' also disappears when this region is liquid filled, to be replaced by a fainter, slightly curving and almost horizontal highlight [the ''curved highlight,'' arrowed in Fig. 3(a), frame 305]. These three lines are the clearest highlight indicators of whether gas or liquid fills the cone. The ''curved highlight'' in addition gives a qualitative assessment of the void fraction present. It is well defined when the void fraction is low (termed ''clear'' water, as seen in Fig. 2, frames 3, 16, 21–22; Fig. 3, frames 25–305). However, when it is high, the strong scatter from this region degrades the curved highlight (i.e., ''bubbly water'' is present at this location in Fig. 2, frames 8, 15, 17; Fig. 3, frame 23). Visual cross checks were regularly performed to ensure stability of the highlights by placing static menisci at varying heights.

Also arrowed in frame 1 is a dark horizontal line, which divides all the frames in half. Lying directly on top of this is a light horizontal line (which is more intense in later frames, e.g., frame 15). This pair forms the ''divisor highlight:'' it represents simply the physical boundary between the PMMA sections of the cone. The upper section is designed to take the cylindrical polycarbonate inserts. Where the aforementioned arrow meets the horizontal dark line in frame 1 corresponds to the left side of the base of the insert, and a vertical highlight above this point demarcates the extreme left edge of the insert [labeled ''edge highlight'' in Fig. 2(b), frame 1].

At this relatively low framing rate it is not possible to see the meniscus clearly during the first collapse. However, its approximate position can be inferred from the highlights. By frame 3 ''clear'' water is present in the lower part of the cone [the bottom highlight has been replaced by the curved highlight, arrowed and labeled in Fig. 2(a) and (b), respectively]. However, the apex highlight remains, implying that the top of the cone contains a coherent gas pocket.

By frame 4 water fills even more of the cone, the apex highlight having disappeared. In fact, frame 4 corresponds to a moment shortly after the first rebound (as can be confirmed

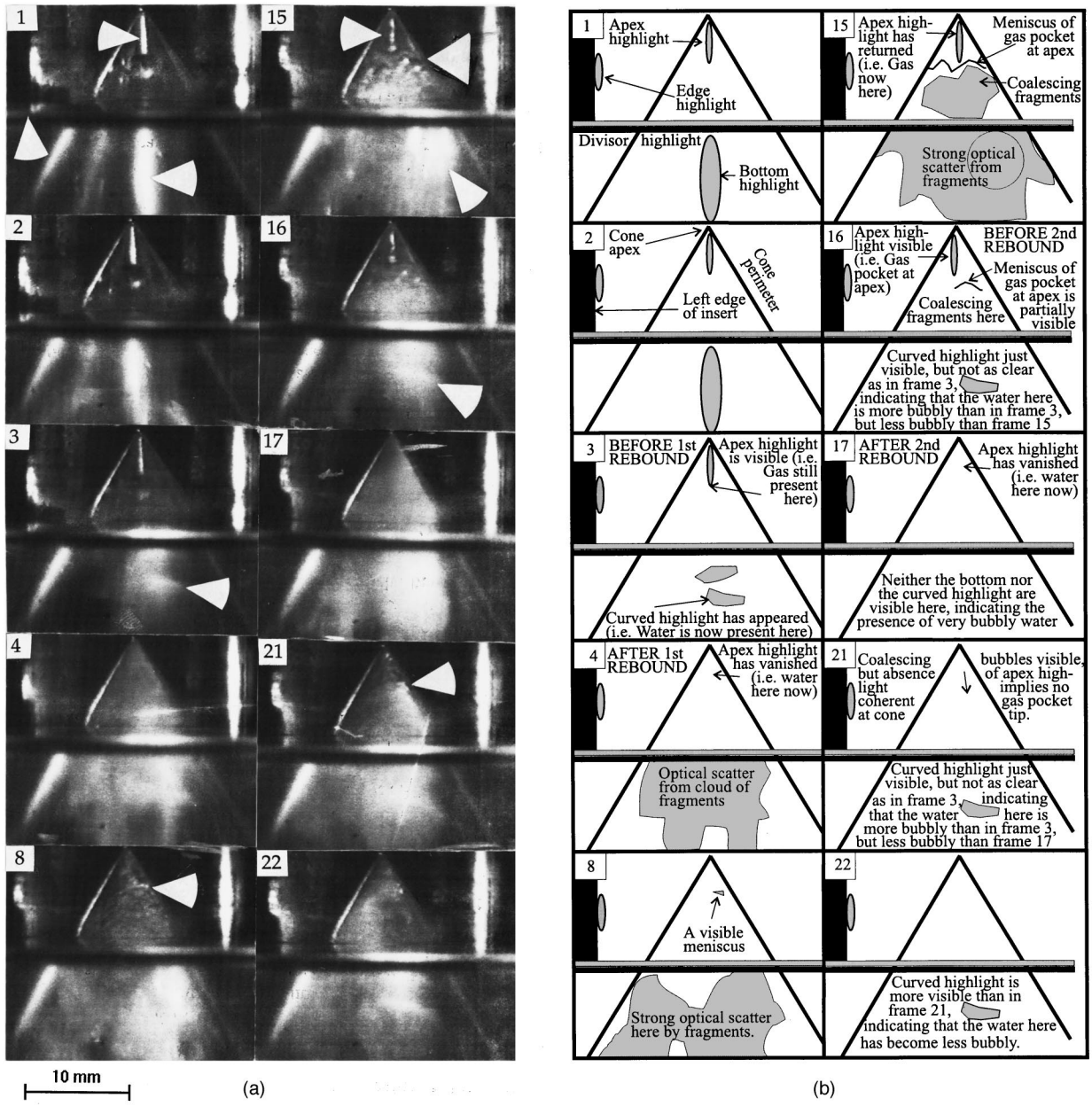

FIG. 2. (a) A selection of 10 frames from a consecutive sequence of 305, filmed at 1000 f.p.s. (each frame occupying full screen). Just prior to collapse the meniscus was $R_i = 60 \pm 5$ mm below the cone tip; after the collapse and subsequent bubble oscillation/fragmentation/coalescence features had ceased, there was a spherical bubble of diameter 2.7 ± 0.05 mm $(= 2R_f)$ remaining close to the cone tip. The device contained 1050 ml of degassed water ($h_i = 37.1$ cm). The arrowed features are described in the text. (b) A frame-by-frame schematic illustration to assist in the identification of features in (a).

through examination of pressure traces—see Sec. II B). A cloud of very small bubbles extends from the cone apex almost to the base of the frame. This interesting feature has been ejected away from the collapse center (the apex) during the rebound. These fragments are clear on the video sequence, but harder to see in still frames, and the cloud outline has been sketched in Fig. 2(b). By frame 8 these fragments have started to coalesce, and a meniscus is visible [arrowed and labeled in Fig. 2(a) and (b), respectively]. This meniscus is simply one feature in a complicated bubble cloud, which is large enough and slow enough to be captured on screen, and there is by no means a single air pocket above it and water below. However, by frame 15 there is clearly a coherent gas pocket at the tip, as opposed to a cloud of bubble fragments, as evidenced by the return of the ''apex highlight'' there [upper arrow, Fig. 2(a)]. The meniscus itself is not flat [middle arrow, Fig. 2(a)], but forming from the coalescence of bubble fragments, which fill much of the water below it [see, for example, the scatter around the lowest arrow of Fig. 2(a)]. These features are drawn schematically on frame 15 of Fig. 2(b). The cloud in the lower half of the cone is continually decreasing in void fraction. Compare, for example, the lower arrowed regions in frames 15 and 16: in the latter, the ''curved highlight'' is again visible, indicating the presence of water without a sufficient density of bubbles to degrade it. The relevant comment in Fig. 2(b) draws attention to the fact that the curved highlight has a clarity

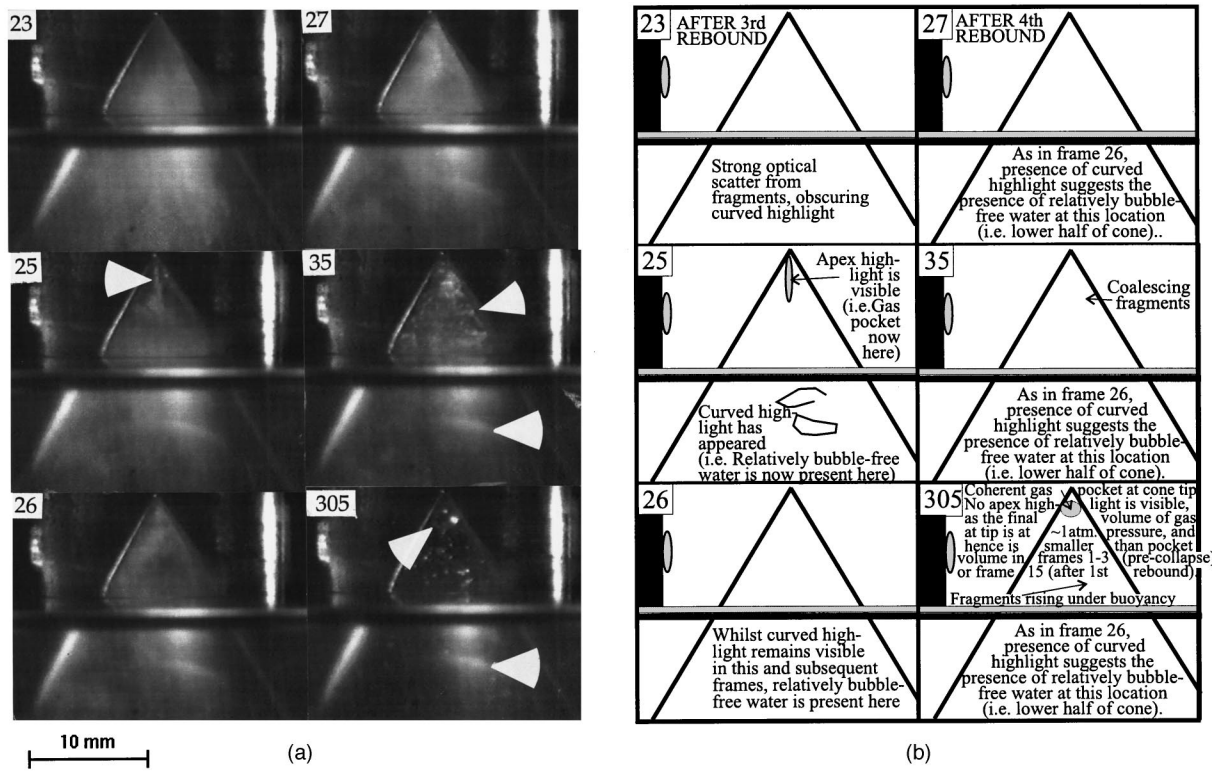

FIG. 3. (a) A selection of 6 further frames from the same consecutive sequence of 305 that is shown in Fig. 2. The arrowed features are described in the text. (b) A frame-by-frame schematic illustration to assist in the identification of features in (a).

intermediate between that found in frames 3 and 15, reflecting the void fractions present.

By frame 17 the second collapse/rebound has occurred (again, see the pressure traces—Sec. II B). The ''apex highlight'' has again disappeared, indicating the loss of a visible coherent gas pocket at the tip. Frames 17 and 21 correspond to similar periods after the second collapse, to those imaged after the first collapse in frames 4 and 8. There are similarities [for example, the menisci arrowed in frames 8 and 21 of Fig. 2(a)]. However, certain differences are clear from the comments in Fig. 2(b). Scatter from a higher void fraction in frame 8 degrades the curved highlight in frame 21.

The third rebound occurs between frames 22 and 23 (Fig. 3). By frame 25 the ''apex highlight'' has returned (arrowed), indicating the presence of a coherent gas pocket at the tip. The void fraction in the water in the lower half of the cone is decreasing, the curved highlight becoming visible in frame 25. It remains visible for the remainder of the film [see lower arrow in Fig. 3(a), frames 35 and 305]. There are two reasons why the void fraction here remains low. First, the progressively weakening rebounds are less able to fragment the tip gas pocket and project the fragments to depth (compare with the decreasing amplitude of the pressure trace in Fig. 6). Second, buoyancy provides a steady force for clearing bubbles from the lower part of the cone.

The fourth rebound occurs just before frame 27. After this one there are no more collapses that eject clouds of bubble fragments from the tip. In frame 35 of Fig. 3(a), the bubble cloud from the fourth collapse is coalescing, and will eventually form the final bubble, the meniscus of which is very faint but indicated by the upper arrow in frame 305.

Having identified the basic form of the collapse/rebound and fragmentation/coalescence cycles, the higher-speed sequences can now be interpreted. Figure 4(a) shows a selection of 60 frames from a consecutive sequence of 4020, filmed at 6000 f.p.s. Each frame occupies $\frac{1}{6}$ screen, the image corresponding to a vertical strip measuring 4 mm×34 mm high. It is presented rotated 90 degrees from true such that the left-hand edge of each image corresponds to a region close to the base of the cone, and the right-hand side of each image corresponds to a region close to the apex of the cone. Indeed, the cone apex is visible near the bottom right corner of each frame, so that the bottom edge of each frame is nearly aligned with the axis of the cone. Figure 4(b) shows a schematic illustration of this high-speed photographic sequence. For clarity, the gray scale in Fig. 4(b) has been inverted to form a negative image.

Arrowed in frame 2 of Fig. 4(a) are a pair of lines, dark and light, which form two of the three bands of the ''divisor highlight.'' This highlight physically corresponds to the boundary between the upper and lower sections of the cone (as arrowed in frame 1 of Fig. 2). These two bands [labeled B2 and B3, respectively, at the bottom left of Fig. 4(b)] are always present. However, the intensity of B3 varies (decreasing, for example, when clouds of bubble fragments scatter its emission, as in frames 23–30 and 55–60).

The third band of the divisor highlight (B1) appears as an intermittent white line in Fig. 4(a). The same is true of the highlight labeled ''*A*'' at the bottom left of Fig. 4(b) [and arrowed in frame 4020 of Fig. 4(a)]. Their appearance can be used to qualitatively distinguish between three states: whether at the location of each there is air, or water having

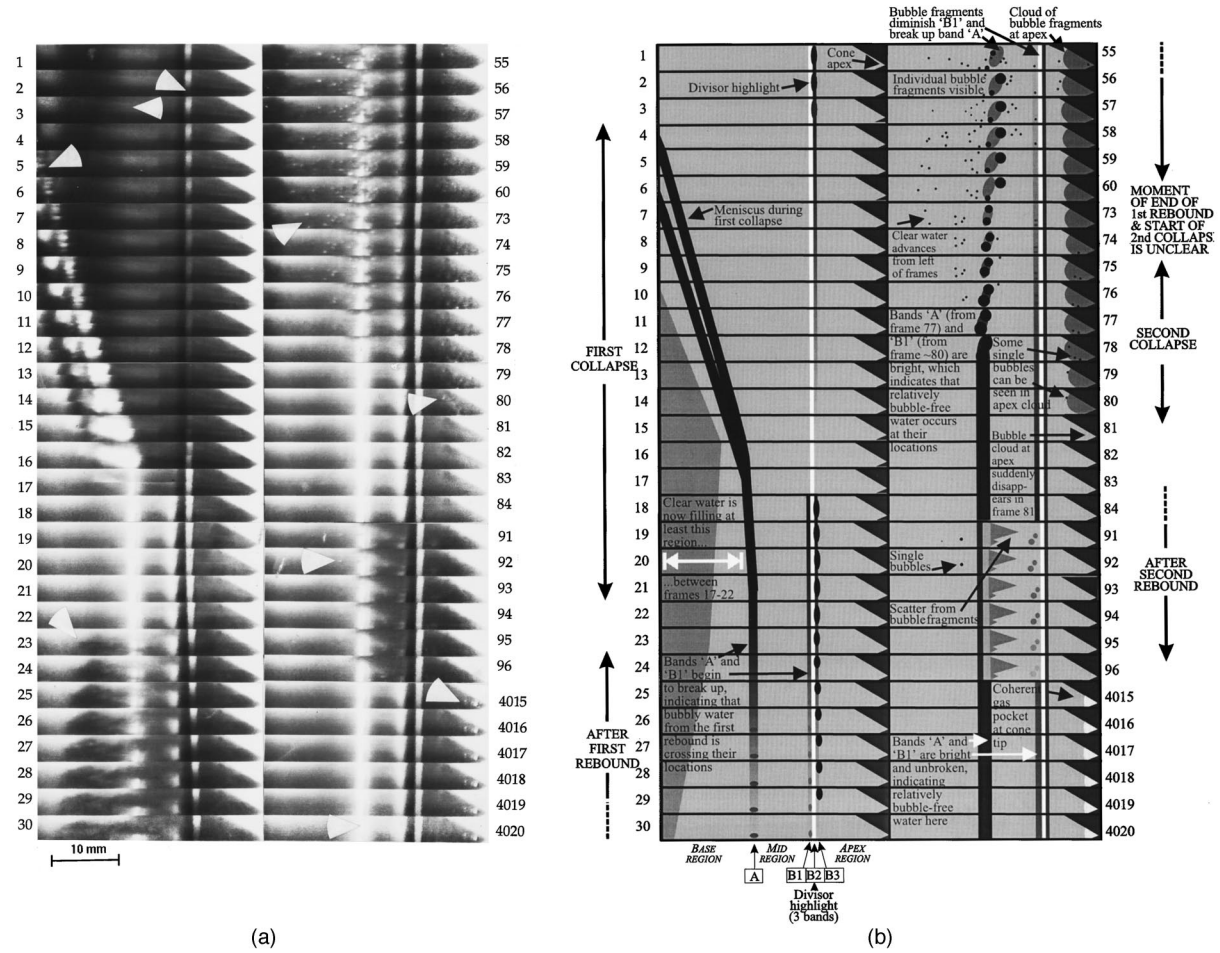

FIG. 4. (a) A selection of 60 frames from a consecutive sequence of 4020, filmed at 6000 f.p.s. Each frame occupies $\frac{1}{6}$ screen, the image corresponding to a vertical strip measuring 4 mm$\times$34 mm high. It is presented rotated 90 degrees from true such that the left-hand edge of each image corresponds to a region close to the base of the cone, and the right-hand side of each image corresponds to a region close to the apex of the cone. Indeed, the cone apex is visible near the bottom right corner of each frame, so that the bottom edge of each frame is nearly aligned with the axis of the cone. Unlike the other arrows in the figure, that in frame 3 does not point to any feature in the image; rather its tip precisely marks the location corresponding to the base of the image frames of Figs. 2 and 3. Just prior to collapse, the meniscus was $R_i = 50 \pm 5$ mm below the cone tip; after the collapse and subsequent bubble oscillation/fragmentation/coalescence features had ceased, there was a spherical bubble of diameter 1.5 ± 0.05 mm$(=2R_f)$ remaining close to the cone tip. The device contained 1050 ml of degassed water ($h_i = 37.1$ cm). The arrowed features are described in the text. (b) A frame-by-frame schematic illustration to assist in the identification of features in (a).

low void fraction (loosely termed ''clear water''), or water of high void fraction (''bubbly water''). When air is present, these bands are not visible (frames 1–17 for B1; frames 1–15 for A). They are intense when clear water is present (frames 18–22, 78–84, and 4015–4020 for both B1 and A). Their appearance is dimmer and broken when bubbly water at their locations scatters the light (frames 23–30, 55–76, and 91–96). Each frame can conveniently be divided into three regions [see labels at bottom left of Fig. 4(b)]. The ''apex region'' occurs between the divisor highlight and the cone tip; the ''mid region'' occurs between bands A and B1; and the base region occurs between band A and the left side of each frame (i.e., physically below band A, since the frames are shown rotated through 90 degrees).

Because of the higher framing rate, it is now possible to capture the image of the meniscus of the collapsing bubble. This appears around frame 5 [arrowed in Fig. 4(a)], and travels up the cone. It is not flat, but instead contains instabilities. The gradient mapped out by the meniscus in frames 5–16 of Fig. 4(a) gives the speed of the bubble wall, and it can readily be seen that this is accelerating (since the locus mapped out by any point on the meniscus follows a curve). From the image, the average speed between frames 6 and 8 is 6.9 ± 0.6 m/s, between frames 9 and 12 it is 8.5 ± 1.9 m/s, and between frames 13 and 15 it is 10.6 ± 2.0 m/s. These values are plotted in Fig. 5 against the solution of Eq. (2).

After frame 16 it is not simple to track the collapsing meniscus. This is because of both optical limitations and the fact that, as it accelerates to greater speeds, it becomes less distinct in the image. However, the intensity and integrity of band A in frames 17–22, and of band B1 in frames 18–21, indicate the presence of clear water. Hence the meniscus has passed these points at these times. The bubble collapses into the cone, the extent of this ''first collapse'' being indicated down the left side of Fig. 4(b). It then rebounds, ejecting a cloud of bubble fragments, which rapidly travels down the cone. This causes bands A and B1 to lose brightness and integrity (frame 23). Measurements of the image of the perimeter of this cloud [arrowed in Fig. 4(a), frame 23] show two features. First, the fragment cloud expands to well below

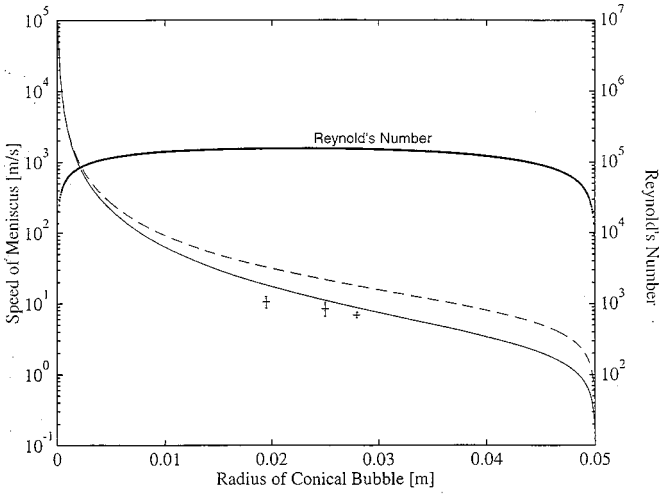

FIG. 5. Plot of meniscus velocity against (i) cone tip-to-meniscus distance for the collapse of a conical bubble containing gas (R_c) [solid, Eq. (2) for $p_{g,i}=12.9$ Pa], (ii) cone tip-to-meniscus distance for the collapse of an empty conical bubble (R_c) [dotted, Eq. (2) for $p_{g,i}=0$ Pa, and, in fact, indistinguishable from (i)], and (iii) bubble radius for the Rayleigh collapse of an empty spherical cavity (R) [dashed, calculated after Rayleigh (Ref. 1)]. The initial conditions are that $R=R_c=50$ mm, $\dot{R}_c=\dot{R}=0$, and $h_i=371$ mm. The fixed apparatus dimensions are given in the text. Also shown are the bubble wall speeds from the data of Fig. 4, and the estimated Reynolds number for the flow in the pipe (see text for the calculation of both).

the base of the images shown in Figs. 2 and 3 [as indicated by the arrow in Fig. 4(a), frame 3]. Second, the images in frames 25–28 suggest that the cloud perimeter is expanding away from the cone apex at 3.5 ± 0.8 m/s. However, details of the underlying optical scatter mean that this velocity should be treated with more caution than the other speeds measured from this film.

The bubble cloud continues to expand away from the cone apex, and during this some coalescence occurs. By frame 55 of Fig. 4, the cone still contains a significant amount of water, at least up to the level of band B1, as both it and band A are visible. However, their integrities are low, the light from both being strongly scattered. Individual bubble fragments are visible throughout the frame [dark points in Fig. 4(b), frame 55 onwards, are placed at the location of the clearest bubbles in Fig. 4(a)]. Note in particular the individual bubbles in the ''base region,'' and the presence of a cloud of bubbly water at the apex.

The indications from numerous video sequences such as this are that, immediately after the first rebound, there is no evidence of a sizeable ''main'' bubble remaining at the cone apex. [As marked in Fig. 4(b), the first rebound starts just before frame 24, and persists until some time after frame 60.] Instead, a cloud of tiny bubble fragments is ejected away from the apex. Coalescence occurs in the cloud, and the system contains ''bubbly water,'' a population of tiny bubbles with radii much smaller than R_f. This is the scenario shown in frames 55–60.

However, by frame 73 the second collapse has started, and the system changes dramatically. The second collapse appears, visually, as the convergence towards the cone apex of the region of ''bubbly water.'' The impression is that the bubble fragments are driven towards the apex. However, in addition to the translation of fragments, there will be a second contribution to this impression: as the local pressure increases, bubble fragments will be compressed, the void fraction will drop, and the water will appear to clear. The advance of a region of clear water from the left in frames 73–76, at 10 ± 6 m/s, can be seen by the progressive disappearance of fragments [Fig. 4(b)]. As a result, band A in frame 77 has become almost as bright as in frame 18, indicating that the water there has a low void fraction.

It is not so simple to see what happens close to the apex. Comparison of this region between frames 1–6 (when the apex is air filled) and frames 55–60 shows that, in the latter period, there appear to be bubble fragments near the apex. As the second collapse progresses, there is evidence of some structuring in the population, and it may be that coalescence occurs. Certainly the region contains a dense, compressing cloud of bubbles, with individual ones visible [one is arrowed in Fig. 4(a), frame 80; the approximate locations of others is indicated by dots in Fig. 4(b)]. The transition from frame 80 to 81 is critical: the apex region suddenly transforms from containing a bubbly cloud, to becoming ''clear'' water (the fragments presumably being compressed to give a low void fraction). The compression of the cloud is clearly rapid (as one would expect at the end of the collapse—see Fig. 5), since this region transforms from ''bubbly'' to ''clear'' in a single frame.

In Fig. 4(a), frames 81–84, bands A and B1 are bright and unbroken, and the cone apex is a clear, light gray: all three locations contain liquid of low void fraction. The same effects can be seen in frames 19–21 for the end of the first collapse. Between frames 84 and 91, the apex region darkens, and bands A and B1 dim and lose integrity. This is identical to the pattern seen at the end of the first collapse in frames 22 and 23 and the ejection/expansion of the bubble cloud from the apex after the second rebound. This ejection is not so energetic, and the cloud does not extend nearly so far from the apex (a very rough impression of the limit is given by the arrow in frame 92). The ''mid'' region contains visible bubble fragments. The cycle repeats, but as the rebounds become less energetic, the fragmentation at rebound is not complete, and eventually there is a coherent gas pocket undergoing small-amplitude oscillations close to the tip (arrowed in frame 4015).

It is interesting to note that, moments after the two rebounds, the images look very similar (frames 23–30 and 84–96) in all three regions (base, mid, and apex). This is because they contain water having similar void fractions. However, this is not the case when comparing the initial collapse (up to frame 21), and the second collapse (frames 71–81). The last four frames of each collapse appear to be very similar in the ''base'' and ''mid'' regions, but have obvious differences at the apex. Interestingly, the same applies for the period long after the collapse (frames 4015–4020). The ''base'' and ''mid'' regions here look very similar to those that occur towards the end of each collapse (frames 17–21 and 79–83), because these regions again contain water having a low void fraction, though for a very different reason: in frames 4015–4020 the fragments are

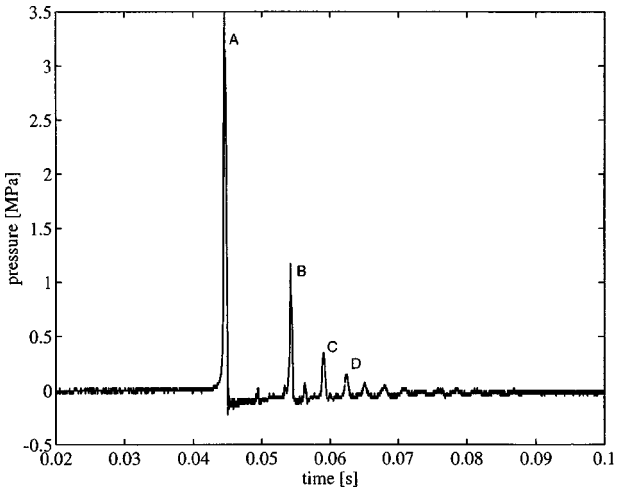

FIG. 6. Plot of a hydrophone signal (triggered at $t=0$) recorded 10 cm below the cone apex. Rebound pressure emissions are labeled: ''*A*'' corresponds to the signal emitted after the first collapse, ''*B*'' to that emitted after the second collapse, and so on. Transient signals between these correspond to reflections of these signals within the pipe (see Ref. 17).

smaller, being at equilibrium with atmospheric pressure.

B. Pressure records

Figure 6 shows the hydrophone record of the pressure in the liquid, measured 10 cm below the cone apex. Time $t=0$ corresponds to the common trigger signal produced by the photon-counting signal in response to the signal from the accelerometer mounted on the top-plate. This trigger signal also causes a single 12 μs flash, which Leighton *et al.*[20] record on high-speed sequences similar to Fig. 4. Comparison of these with simultaneous pressure traces allows the identification of the time at which, during each collapse, the bubble achieves minimum size, and the moment (a short time later) when the rebound pressure signal is detected by the sensor placed 10 cm below the bubble. The interval between the two can be used to give an estimate of the spatially averaged sound speed in the liquid between the bubble wall and the hydrophone. This is done in Table I for the first, second, and third rebounds, for a range of precollapse (R_i) and final (R_f) bubble sizes.

These figures can also be used to estimate the collapse times and compare these with theory, as obtained by integration of Eq. (2) described in Sec. I B. There are two ways of estimating the collapse time. First, the pressure sensor used by Leighton *et al.*[17] makes it possible to observe the passage over the pressure sensor of the pressure wave caused by the opening of the plate (see, as an example, their Fig. 4). From the interval between this and the measurement of the rebound pressure on the same sensor, it is possible to estimate the collapse time. However, quantifiable error arises both because, since the rebound pressure pulse saturated the pressure sensor, the signal was clipped and there was some uncertainty in the position of the pulse apex; and because, to correct for the travel time of the rebound pulse, a propagation speed must be assumed, which is by no means obvious (Table I). Second, high-speed images can be used. However, in the images presented in this paper, only the time between

TABLE I. The sound speed in the cone during the first, second, and third rebounds for various sizes of R_i and R_f. It was calculated from the time difference between the instant at which the bubble radius is a minimum (as measured from the high-speed video recording) and when the rebound pressure wave reaches the hydrophone.

Initial and final bubble sizes		(Sound speed/ m/s)$\pm$60 m/s		
$R_i\pm5$ mm	$R_f\pm0.05$ mm	First rebound	Second rebound	Third rebound
55	2.00	200	215	195
60	1.40	230	255	160
50	0.90	180	220	140
55	1.10	290	290	160
55	1.10	355	···	···
55	1.00	300	185	130
60	1.10	290	280	270

rebounds is directly observable. The initial collapse time can be extrapolated back from the inter-rebound times using the geometric series factor by which the inter-rebound collapse times decrease in duration as a result of damping.[24] This is clearly an approximation, given that from the images it is clear that fragmentation occurs. Using a different symbol for each, these two methods are used to estimate collapse times and compare with the predictions of Eq. (3) for a gas-filled conical bubble (Fig. 7). Also plotted, for comparison, is the collapse time of an empty spherical cavity, following Rayleigh.[1]

In the above data, and that of Sec. II C, the insert used retains the conical geometry right up to the cone apex. For the data of Fig. 8, that insert is replaced by the one that truncates the cone 5.25 mm below the apex, forming a horizontal window of 6.05-mm diameter over which the spatially averaged pressure can be monitored. The technique is detailed in Leighton *et al.*[18] who presented preliminary results. Figure 8 shows a larger set of results for the pressures generated by the first collapse, and compares the measurements

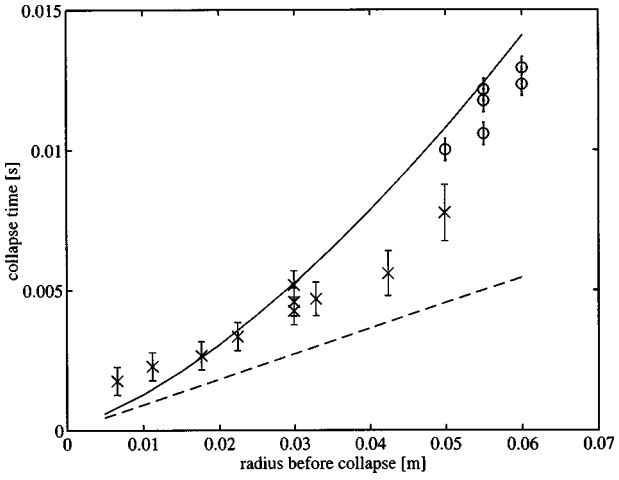

FIG. 7. Plots of the collapse time of (i) a gas-filled conical bubble [solid, found through integration of Eq. (2) using Eq. (3)] and (ii) an empty spherical Rayleigh cavity (dashed). The estimates of collapse times from data are shown, calculated from records of the pressure in the liquid ($\times$), and from extrapolation from the high-speed images of the rebounds ($\bigcirc$). In all the collapses from which these measurements were taken $R_f=0.95\pm0.05$ mm and the device contained 1050 ml of degassed water ($h_i=37.1$ cm).

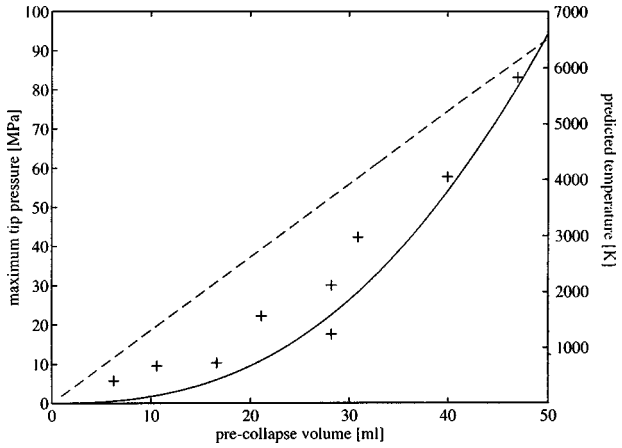

FIG. 8. Measurements of pressure taken at the top of a cone that has been truncated 5.25 mm below the normal position of the apex. The measurements are spatially averaged across the cross section at the position of the sensor. Predictions of theory for pressure are shown [Eq. (7), solid line]. Also shown are predicted temperatures that would occur under these conditions [Eq. (8), broken line]. The device contained 1050 ml of degassed water; the pregrowth bubble volume was 0.9 ml.

with those of theory [Eq. (7)]. The comparison is remarkably good, considering the assumptions of the theory. It is noted, however, that the latter assumes homogeneous conditions within the gas, and the measurement is spatially averaged over the sensor, which might artificially assist the fit. Although there are no measurements of the temperature in the device, given the degree of agreement in the pressure data, it was felt useful to show in Fig. 8 the gas temperatures predicted by theory [Eq. (8)]. Although in the absence of measurement this is by no means meant to indicate a belief that the thermal conditions within the bubble are homogeneous, the results are of interest given the role of such thermal criteria.[25–27]

C. Measurements of sonoluminescence[28]

Figure 9 shows a sequence of six frames from the CCD video. The vertical edges of the cone tip insert and the tip of the cone itself are marked with arrows in frame 4. Sonoluminescence is clearly visible in frames 3 and 4. The sonoluminescence does not appear to occur at the tip of the cone, but a few millimeters below the tip, and off center. A similar asymmetry was observed by Leighton *et al.*[16] Since the exposure per frame is around 40 ms (see Sec. I A), which is greater than the inter-rebound time, and there is finite persistence associated with the display, it requires better time resolution to determine the role of sonoluminescence in the time history of the collapse cycle. This is provided in Fig. 10 by the output of the photon counter, which is a histogram showing the number of photons per 0.1-ms interval. It records a single peak of 120 photons in the 0.1 ms associated with the end of the first collapse (as is evident from the simultaneous hydrophone trace, $t=0$ corresponding to the receipt of the trigger signal for both). The luminescence output at other times is within the noise. Given that the light detector has an active area of 1 mm^2 and a photon detection efficiency of $40\%\pm10\%$, that it is placed 50 mm from the cone tip, and

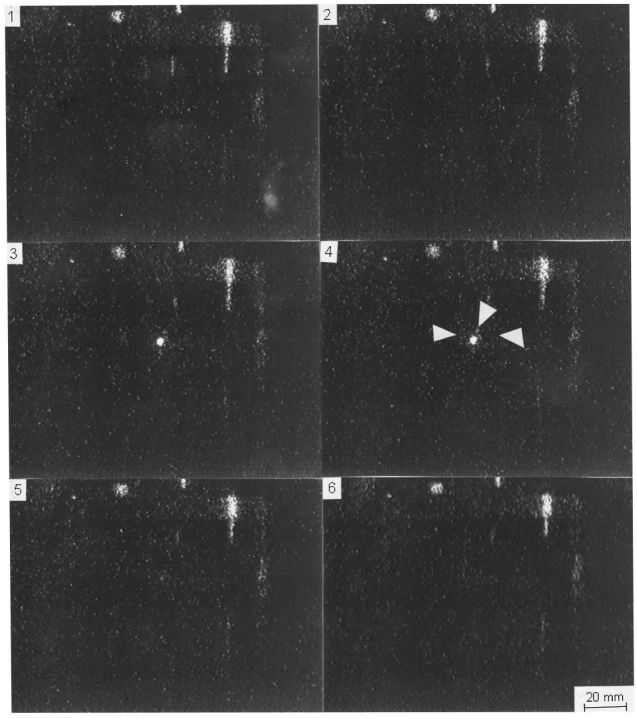

FIG. 9. A sequence of six frames from the CCD video. Exposure per frame is around 40 ms (see Ref. 18). Time-independent features are reflections of ambient low-level illumination from the insert. Just prior to collapse, the meniscus was $R_i=60\pm5$ mm below the cone tip; after the collapse and subsequent bubble oscillation/fragmentation/coalescence features had ceased, there was a spherical bubble of diameter 2 ± 0.05 mm ($=2R_f$) remaining close to the cone tip. The device contained 1050 ml of degassed water ($h_i=37.1$ cm). These frames correspond to the plots shown in Fig. 10.

that the PMMA absorbs $45\%\pm5\%$ of the photons which are generated at the apex, then the sonoluminescence flash contained $(2\pm0.5)\times10^7$ photons.

III. DISCUSSION AND CONCLUSIONS

Simple apparatus has been produced which generates the unstable collapse of a gas pocket. The bubble size prior to

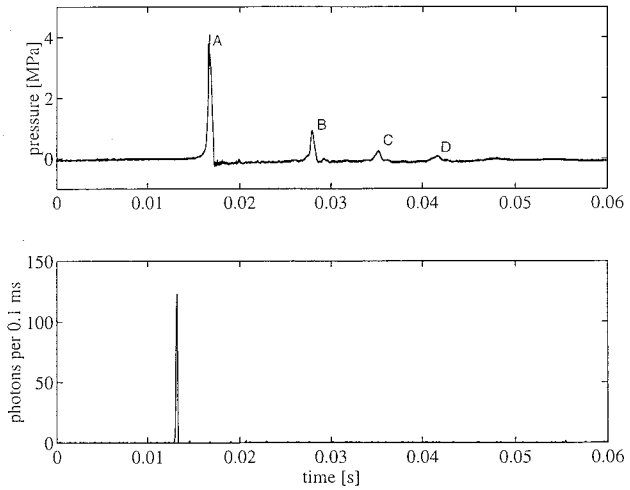

FIG. 10. Simultaneous records of (a) the hydrophone and (b) the photon counter, which is a histogram showing the number of photons per 0.1-ms interval. The datum $t=0$ corresponds to the receipt of the trigger signal for both traces. These plots correspond to the frames shown in Fig. 9.

growth, the size prior to the first collapse, and the inertia associated with the collapse can all be readily controlled. The pressure in the liquid (and, to a certain extent, the gas) can be monitored, and estimates made of the sound speed close to the bubble wall. The collapse can be photographed and the sonoluminescence imaged and quantified, and in all the records has only been produced by the first collapse. The bubble fragments after the first collapse, and the ''rebound'' appears to be in the form of an expanding cloud of bubble fragments. These coalesce during the subsequent collapse phase, and hence the bubble pressure trace resembles that which would be expected from the simple model of a single bubble, expanding and rebounding with decreasing amplitude until, at the end, one can observe a single bubble undergoing linear pulsations. A number of observations (wall speed, collapse time, and gas pressure) have been compared with a theory, adapted from Rayleigh, Noltingk, and Neppiras, based on initial isothermal bubble growth followed by adiabatic collapse.

ACKNOWLEDGMENTS

The conical bubble work described here and previously[17,18,20] has progressed unfunded through student projects. As such it would not have proceeded without the indulgence of the host laboratories in which I supervised the work (Cavendish Laboratory and the ISVR), and without the technical support of Ray Flaxman and Dave Johnson who constructed the apparatus on zero budget. I am also grateful to Dr. A. D. Fitt for suggestions on integration routines, and to the Engineering and Physical Sciences Research Council (GR/M24615) for the loan of the high speed camera. I am very grateful to Dr. P. R. Birkin for excellent discussions.

[1] Lord Rayleigh, ''On the pressure developed in a liquid during the collapse of a spherical cavity,'' Philos. Mag. **34**, 94–98 (1917).
[2] B. E. Noltingk and E. A. Neppiras, ''Cavitation produced by ultrasonics,'' Proc. Phys. Soc. London, Sect. B **63**, 674–685 (1950).
[3] E. A. Neppiras and B. E. Noltingk, ''Cavitation produced by ultrasonics: Theoretical conditions for the onset of cavitation,'' Proc. Phys. Soc. London, Sect. B **64**, 1032–1038 (1951).
[4] W. H. Besant, *A Treatise on Hydrostatics and Hydrodynamics* (Deighton, Bell, London, 1859), p. 158.
[5] C. C. Wu and P. H. Roberts, ''Shock-wave propagation in a sonoluminescing gas bubble,'' Phys. Rev. Lett. **70**(22), 3424–3427 (1993).
[6] W. C. Moss, D. B. Clarke, W. White, and D. A. Young, ''Hydrodynamic simulations of bubble collapse and picosecond sonoluminescence,'' Phys. Fluids **6**, 2979–2985 (1994).
[7] D. F. Gaitan and L. A. Crum, ''Observation of sonoluminescence from a single cavitation bubble in a water/glycerine mixture,'' in *Frontiers of Nonlinear Acoustics*, 12th ISNA, edited by M. F. Hamilton and D. T. Blackstock (Elsevier, New York, 1990), p. 459.
[8] B. P. Barber, R. Hiller, K. Arisaka, H. Fetterman, and S. Putterman, ''Resolving the picosecond characteristics of synchronous sonoluminescence,'' J. Acoust. Soc. Am. **91**, 3061–3063 (1992).
[9] L. A. Crum and S. Putterman, ''Sonoluminescence,'' J. Acoust. Soc. Am. **91**, 517 (1992).
[10] L. A. Crum and S. Cordry, ''Single-bubble sonoluminescence,'' in *Bubble Dynamics and Interface Phenomena*, Proc. IUTAM Symposium, Birmingham, UK, 6–9 September 1993, edited by J. R. Blake, J. M. Boulton-Stone, and N. H. Thomas (Kluwer Academic, Dordrecht, 1994), pp. 287–297.
[11] T. Lepoint, N. Voglet, L. Faille, and F. Mullie, ''Bubbles deformation and interface distortion as a source of sonochemical and sonoluminescent activity,'' in *Bubble Dynamics and Interface Phenomena*, Proc. IUTAM Symposium, Birmingham, UK, 6–9 September 1993, edited by J. R. Blake, J. M. Boulton-Stone, and N. H. Thomas (Kluwer Academic, Dordrecht, 1994), pp. 321–333.
[12] C. Eberlein, ''Sonoluminescence as quantum vacuum radiation,'' Phys. Rev. Lett. **76**, 3842 (1996).
[13] A. P. Prosperetti, ''A new mechanism for sonoluminescence,'' J. Acoust. Soc. Am. **101**, 2003–2007 (1997).
[14] T. J. Matula and R. A. Roy, ''Optical pulse width measurements of sonoluminescence in cavitation-bubble fields,'' J. Acoust. Soc. Am. **101**, 1994–2002 (1997).
[15] T. G. Leighton, P. R. White, and M. A. Marsden, ''Applications of one-dimensional bubbles to lithotripsy, and to diver response to low frequency sound,'' Acta Acust. **3**, 517–529 (1995).
[16] Simple theory predicts that increasing the inertia (by, for example, lengthening the tube) will not affect the minimum volume attained. However, it will reduce the bubble wall speed during collapse. Slower speeds will have important implications regarding the occurrence of meniscus fragmentation and shocks, and the thermodynamics of the collapse.
[17] T. G. Leighton, W.-L. Ho, and R. Flaxman, ''Sonoluminescence from the unstable collapse of a conical bubble,'' Ultrasonics **35**, 399–405 (1997).
[18] T. G. Leighton, A. D. Phelps, B. T. Cox, and W.-L. Ho, ''Theory and preliminary measurements of the Rayleigh-like collapse of a conical bubble,'' Acta Acust. **84**(6), 1014–1024 (1998).
[19] P. G. Kosky and G. A. Henwood, ''A new technique for investigating vapour bubble implosion experimentally,'' Br. J. Appl. Phys. **2**, 630–634 (1969).
[20] T. G. Leighton, B. T. Cox, P. R. Birkin, and T. Bayliss, ''The Rayleigh-like collapse of a conical bubble: Measurements of meniscus, liquid pressure, and electrochemistry,'' in *Proceedings of the 137th Regular Meeting of the Acoustical Society of America and the 2nd Convention of the European Acoustics Association (Forum Acusticum 99, integrating the 25th German Acoustics DAGA Conference)*, March 1999, Paper 3APAB_1.
[21] P. Hawtin, G. A. Henwood, and R. A. Huber, ''On the collapse of water vapour cavities in a bubble analogue apparatus,'' Chem. Eng. Sci. **25**, 1197–1209 (1970).
[22] T. G. Leighton, *The Acoustic Bubble* (Academic, London, 1994), Figure 2.8, §2.1.3b(iii).
[23] B. S. Massey, *Mechanics of Fluids* (Van Nostrand Reinhold, London, 1970), 2nd ed., Chap. 7.
[24] This assumes that the growth and collapse phases of the bubble are symmetrical in time profile. Although it is assumed that the first growth phase, performed here with the vacuum pump, is slow and hence isothermal, the subsequent growth phases can be assumed to be adiabatic, making the assumption of symmetric time profiles after the first rebound not unreasonable. See, for example, Fig. 16 in C. C. Church, ''A theoretical study of cavitation generated by an extracorporeal shock wave lithotripter,'' J. Acoust. Soc. Am. **86**, 215–227 (1989).
[25] C. K. Holland and R. E. Apfel, ''An improved theory for the prediction of microcavitation thresholds,'' IEEE Trans. Ultrason. Ferroelectr. Freq. Control **36**, 204–208 (1989).
[26] R. E. Apfel and C. K. Holland, ''Gauging the likelihood of cavitation from short-pulse, low-duty cycle diagnostic ultrasound,'' Ultrasound Med. Biol. **17**, 179–185 (1991).
[27] American Institute Of Ultrasound In Medicine/National Electrical Manufacturers Association (AIUM/NEMA), *Standard for real-time display of thermal and mechanical indices on diagnostic ultrasound equipment* (AIUM/NEMA, 1992).
[28] One reviewer made a very interesting point, which (with permission) I quote: ''I object very strongly to the use of the word sonoluminescence in section IIC, as the results here refer to nothing like what a normal reader would assume, given the excitement of the last few years about (true) sonoluminescence. There is no 'sono,' only luminescence here.'' To begin on a light note, first-time users of the device are unfailingly startled by the ''bang'' that accompanies the opening of the top plate (which generates the pressure pulse that causes the bubble to collapse). However, the absence of a conventional driving acoustic field, to which the reviewer refers, was also addressed in the review ''Sonoluminescence'' by A. J. Walton and G. T. Reynolds [Adv. Phys. **33**(6), 595–660 (1984)]. They state: ''Harvey (1939) introduced the name *sonoluminescence* (SL) for the luminescence caused by the sound field. A more apposite name might be 'cavitation luminescence,' since the light emission is associated with the presence of suitable size bubbles within the liquid...The appropriate cavitation conditions required for light emission can also be realized by flowing the liquid through a Venturi tube..., by impacting a water jet onto a stationary plate..., by focusing a pulsed laser beam into the liquid..., by

passing a spark discharge through the liquid...and even by smashing thin-walled glass spheres containing low pressure gas under water.'' As a final note, it would, in principle, be possible to generate even single-bubble sonoluminescence without the use of an acoustic field, using a noninertial frame to generate a stable oscillatory pressure field after the manner of T. G. Leighton, M. Wilkinson, A. J. Walton, and J. E. Field, ''The forced oscillations of bubbles in a simulated acoustic field,'' Eur. J. Phys. **11**, 352–358 (1990).